

## Pion-nucleus inelastic scattering at 80 MeV

M. Blecher, K. Gotow, and R. Ng

*Virginia Polytechnic Institute and State University, Blacksburg, Virginia 24061*

R. L. Burman, R. Carlini, S. Dam, M. V. Hynes, M. J. Leitch, and V. Sandberg

*Los Alamos National Laboratory, Los Alamos, New Mexico 87545*

R. Auble, F. E. Bertrand, E. E. Gross, F. E. Obenshain, and J. Wu

*Oak Ridge National Laboratory, Oak Ridge, Tennessee 37838*

G. S. Blanpied, B. M. Freedom, and B. G. Ritchie

*University of South Carolina, Columbia, South Carolina 29208*

W. Bertozzi, M. A. Kovash, and R. P. Redwine

*Massachusetts Institute of Technology, Cambridge, Massachusetts 02139*

(Received 21 December 1981)

80 MeV positive and negative pions inelastically scattered from targets of  $^{12}\text{C}$  and  $^{40}\text{Ca}$  have been studied at laboratory angles between  $50^\circ$  and  $120^\circ$ . Angular distributions are presented for scattering from the 4.44 MeV ( $2^+$ ) state in  $^{12}\text{C}$ , the 3.7 MeV ( $3^-$ ), 13.4 MeV, and 17.5 MeV states in  $^{40}\text{Ca}$ . The cross sections are compared with distorted wave calculations using potentials obtained from elastic scattering.

[NUCLEAR REACTIONS  $^{12}\text{C}(\pi, \pi')$ ,  $^{40}\text{Ca}(\pi, \pi')$ ,  $E=80$  MeV; measured  $\sigma(\theta)$  for low lying ( $^{12}\text{C}$ ,  $^{40}\text{Ca}$ ) and giant resonance ( $^{40}\text{Ca}$ ) states; DWBA analysis.]

## INTRODUCTION

The different properties of the pion ( $\pi$ ) and nucleon ( $N$ ) make the  $\pi$  an interesting alternative strongly interacting nuclear probe. For example, at energies well below the (3,3) resonance the pion-nucleon ( $\pi N$ ) interaction is weak. As a result low energy  $\pi$ 's penetrate to the nuclear interior in pion-nucleus ( $\pi A$ ) reactions. Elastic scattering data at energies  $\leq 80$  MeV (Refs. 1–8) have revealed that the nuclear medium profoundly affects the  $\pi N$  interaction. The data can be parametrized by a first order optical potential, but the potential parameters are not simply related to the free  $\pi N$  amplitudes.

Inelastic  $\pi A$  scattering to specific final states provides an additional test for theoretical models. The inelastic cross sections may be sensitive to parts of the reaction mechanism missing from the first order optical potential which is derived primarily from elastic scattering data, and new nuclear structure effects which exploit other properties of the  $\pi$  may be investigated. For example, the isovector nature of

the  $\pi$  allows studies of both isoscalar and isovector nuclear transitions,<sup>9</sup> and the isospin dependence of giant resonance excitations via  $\pi^\pm$  comparisons.<sup>10,11</sup> These studies are made more interesting by the fact that the ratio of the isospin  $\frac{3}{2}$  to isospin  $\frac{1}{2}$   $\pi N$  amplitudes can be widely varied by appropriate choices of energy.

A considerable amount of data for inelastic scattering to specific final states already exists.<sup>10,12–14</sup> However, most of the data lie in the energy region of the (3,3) resonance. At lower energies (35 to 68 MeV) most of the data are for  $\pi^+$  excitation of the 4.44 MeV ( $2^+$ ) state in  $^{12}\text{C}$ . The bulk of all the data indicates that the distorted wave impulse approximation approach qualitatively explains observed cross sections for collective low lying states.<sup>10,14</sup>

Observation of giant resonance excitation with  $\pi$ 's is clearly established in the (3,3) resonance region,<sup>15</sup> but no clear evidence for such excitation exists at low energies. For  $\pi$ 's between 50 and 100 MeV there are indications for the excitation of a gi-

ant  $E2$  resonance with a rapidly varying energy dependence<sup>16</sup> and for a high-lying state with excitation energy  $\sim 13$  MeV (Ref. 17) in  $^{40}\text{Ca}$ .

We have initiated a program to expand the inelastic scattering data in the energy range from 50 to 100 MeV. In this region the rapid change of the  $\pi N$  amplitudes is well suited for studies of isospin effects and optical potentials used in distorted wave calculations. Even for  $N=Z$  nuclei  $\pi^\pm$  comparisons are important in studying isospin effects in the reaction mechanism, because the nucleus attracts  $\pi^-$  (repels  $\pi^+$ ) such that the scattering occurs at higher (lower) effective energies closer to (farther from) the (3,3) resonance. Thus the importance of the  $I=\frac{3}{2}$   $\pi^+p$  interaction is diminished.

Reported here are angular distributions for 80 MeV  $\pi^\pm$  inelastic scattering to the 4.44 ( $2^+$ ) state in  $^{12}\text{C}$  and the 3.7 MeV ( $3^-$ ) state in  $^{40}\text{Ca}$ . Also reported are  $\pi^+$  angular distributions for excitation of a giant quadrupole resonance at 17.5 MeV and a high-lying state at 13.4 MeV in  $^{40}\text{Ca}$ , including a  $\pi^\pm$  comparison of these excitations at two large scattering angles.

### EXPERIMENTAL METHOD

The experiment was performed on the low energy pion (LEP) channel at the Clinton P. Anderson Meson Physics Facility (LAMPF). A magnetic spectrometer (Fig. 1) was used to momentum analyze pions. The spectrometer is a double-

focusing, broad-range device originally used at the Florida State University tandem Van de Graaff facility.<sup>18</sup> It was rebuilt at LAMPF with the installation of new coils and an increase in pole gap from 2.5 to 5.0 cm in order to increase the effective solid angle.

Pions were detected in a multiwire vertical drift chamber (VDC) capable of measuring both position and angle. The VDC based on an MIT design<sup>9</sup> consists of a grounded plane of field shaping and sense wires between two high voltage planes. Thus a drift cell around each sense wire with the electric field configuration illustrated in Fig. 1 is obtained. Charged particles traversing the chamber cause ionization of the chamber gas (50% argon, 50% isobutane) and the resulting electrons drift with known velocity  $v_d$  along the electric field lines to a sense wire. A delay line method analogous to that described in Ref. 19 was used to determine which drift cells were traversed by the charged particle and to measure the drift time  $\tau_d$  and thus the drift distance  $v_d\tau_d$  in each of these cells. From this information the position of the particle at the wire plane and the angle of the particle's trajectory with respect to the wire plane could be determined.

The main differences between our VDC and the MIT VDC are a large active area ( $135 \times 22.5$  cm), approximately twice as long as the MIT chamber, and use of 14 delay lines rather than three. The large active area made it possible to observe, at 80 MeV, excitation energies up to  $\sim 40$  MeV with a

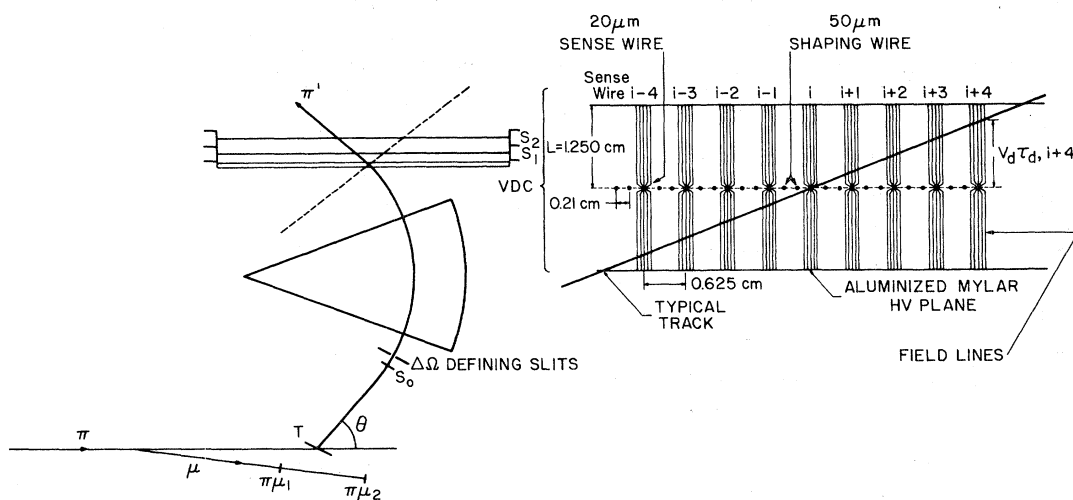


FIG. 1. Experimental setup:  $S_0$ ,  $S_1$ , and  $S_2$  are scintillation counters which in coincidence defined a scattered pion.  $\pi\mu_1$  and  $\pi\mu_2$  are scintillation counters which provided a relative monitor. VDC is a multiwire vertical drift chamber which provided a position (momentum) measurement of scattered pions. Note blow up of the VDC illustrating its construction and principle of operation.

single magnetic field setting. The MIT chamber was designed for experiments in which particles of interest would cross three drift cells. Trajectories were generated by straight line fits to three points. In this experiment inelastically scattered  $\pi$ 's could traverse as many as 14 drift cells (see Fig. 1). Our VDC was able to sample up to 14 points which enabled the omission of those resulting from small drift times. Such points made the largest contributions to the  $\chi^2$  error for the straight line fits. A spatial resolution of  $\pm 0.17$  mm was achieved. In addition,  $\Delta\theta/\theta$ , where  $\theta$  is the angle of the particle's trajectory with respect to the wire plane, was determined to an accuracy of  $\pm 1.2\%$ .

Scintillation counters  $S_0$ ,  $S_1$ , and  $S_2$  in coincidence provided an event trigger.  $S_0$  reduced background from nontarget related events. Pulse heights in  $S_1$ ,  $S_2$  and time of flight between  $S_0$ ,  $S_1$  and  $S_0$ ,  $S_2$  were recorded for each event.  $S_1$  and  $S_2$  had phototubes on each end which permitted a crude ( $\pm 5$  cm) position measurement in the bend direction. Since the VDC determined only the magnitude of the angle of the track, a spurious event indicated by the dashed line in Fig. 1 yielded the same momentum and angle as a  $\pi$  event. However, the additional position measurements in  $S_1$  and  $S_2$  determined the sign of the angle and such spurious events could be rejected.

Relative normalization was provided by two small scintillators  $\pi\mu_1$  and  $\pi\mu_2$  which viewed muons ( $\mu$ ) from  $\pi \rightarrow \mu\nu$  decay in the beam. These counters were mounted at an angle well inside the Jacobian cone, so that the variation of  $\mu$  intensity with angle was small. The relative solid angle was obtained by  $\pi^+$  elastic scattering at fixed energy and angle from a  $^{12}\text{C}$  target for various magnetic field settings, which placed the elastic peak at different positions on the focal plane. Absolute normalization was obtained by measuring the  $\pi^\pm p \rightarrow \pi^\pm p$  cross sections with a  $\text{CH}_2$  target. The  $\pi^+$  cross sections were compared with measured cross sections<sup>20</sup> while the  $\pi^-$  cross sections were compared with phase shift predictions.<sup>21</sup>  $\pi N$  scattering data were taken at a number of different angles. The shape of the angular distribution was consistent with the results of Refs. 20 and 21.

### DATA ANALYSIS

A typical experimental spectrum for scattering from  $^{12}\text{C}$  is shown in Fig. 2. Our overall energy resolution is  $\sim 1.5$  MeV which is sufficient to

separate scattering from the first excited state (4.44 MeV,  $2^+$ ) from other final states. Several spectra for scattering from  $^{40}\text{Ca}$  are shown in Fig. 3. Our energy resolution does not permit us to distinguish between scattering from the 3.7 MeV ( $3^-$ ) and the 3.9 MeV ( $2^+$ ) states. However, fits (see below) to the cross section indicate essentially all  $3^-$  excitation.

Also indicated in Fig. 3 are broad excitations at  $13.4 \pm 0.2$  MeV and  $17.5 \pm 0.2$  MeV with widths of  $2.0 \pm 0.2$  MeV and  $5.1 \pm 1.3$  MeV, respectively. Fits to the spectra assuming only one peak were consistently poorer than for two peaks. The straight line backgrounds shown were used to extract final cross sections. Owing to the poor statistics, variation in the background shape did not produce cross sections in disagreement with those presented here. The 17.5 MeV excitation has been observed with pions at higher energies.<sup>15</sup> It is taken to be mainly a giant quadrupole excitation seen with other strongly interacting probes.<sup>22</sup> These states were also observed with  $\pi^-$  at two angles in this experiment, and the spectra were found to be similar. It is apparent that at these low pion energies the number of events due to high-lying state excitation is quite small relative to the number of events due to other nuclear processes plus background muons which result from the decay of scattered pions. Such behavior is expected at this relatively low energy where the  $\pi N$  interaction is weak and the  $\pi$  must transfer  $\sim 44\%$  of its momentum to the nucleus. The state at excitation energy 13.4 MeV is broad enough to be considered a giant resonance excitation and has not been seen in  $\pi$  scattering data, although there was a hint of its existence in a previous experiment.<sup>17</sup>

Laboratory cross sections for inelastic scattering

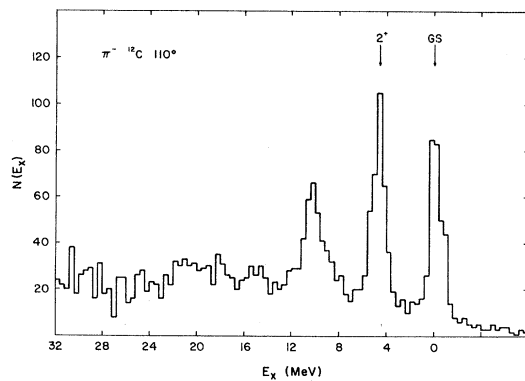


FIG. 2. Energy of scattered pions versus number scattered at  $\theta_{\text{lab}} = 110^\circ$  for a  $^{12}\text{C}$  target.

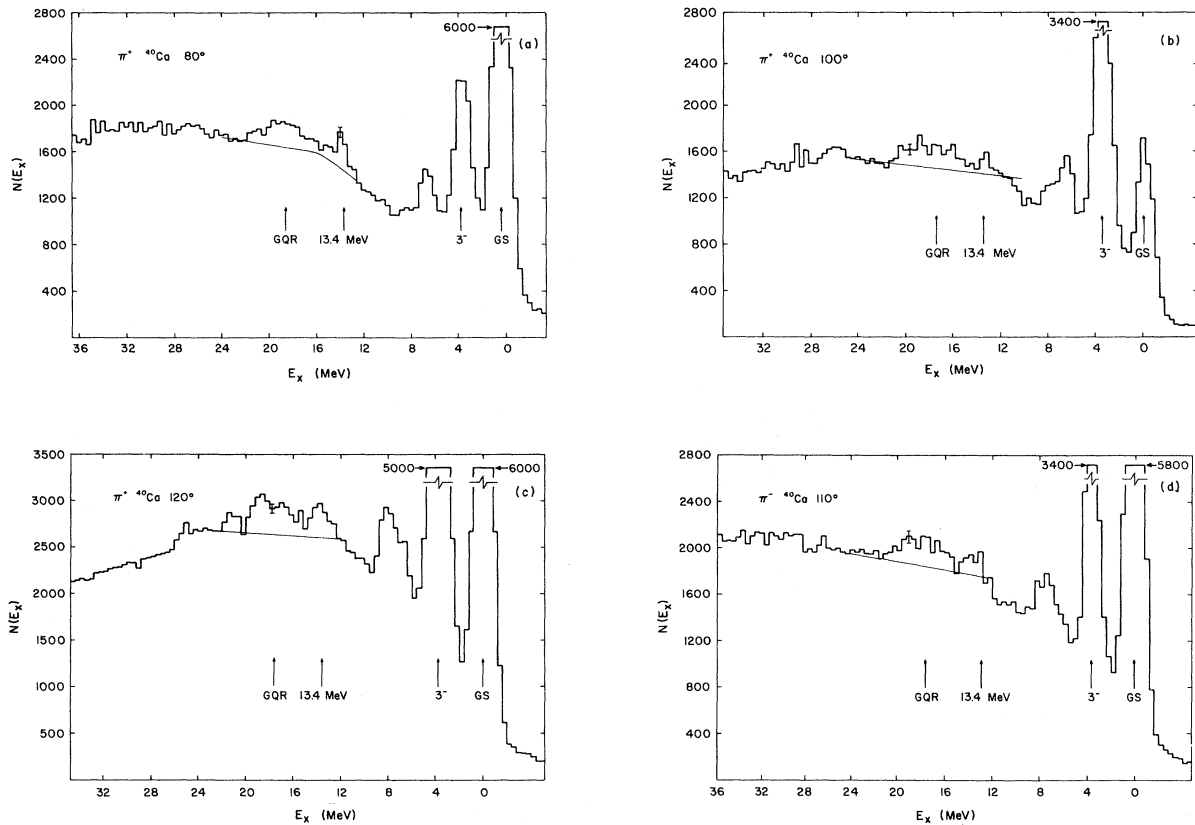


FIG. 3. Spectrum of pions scattered from  $^{40}\text{Ca}$ : (a),  $\pi^+$  at  $\theta_{\text{lab}}=80^\circ$ ; (b)  $\pi^+$  at  $\theta_{\text{lab}}=100^\circ$ ; (c)  $\pi^+$  at  $\theta_{\text{lab}}=120^\circ$ ; (d),  $\pi^-$  at  $\theta_{\text{lab}}=110^\circ$ .

from states with excitation energies  $E_x$  at angle  $\theta$  were obtained from

$$\frac{d\sigma}{d\Omega}(E_x, \theta) = N_x / (Nnt\alpha),$$

where

$N_x$  = the area of the Gaussian fit to the number of counts in the peak of interest corrected for pion decay and relative solid angle.

$N$  = the number of counts in the relative monitor.

$n$  = the density of target nuclei ( $\text{cm}^{-3}$ ).

$t$  = the effective target thickness (cm).

$\alpha$  = the product of the solid angle, the efficiency, and the ratio of pions on target to counts in the relative monitor as determined from our  $\pi^\pm p \rightarrow \pi^\pm p$  measurements.

The inelastic cross sections in the center of mass system are listed in Table I. The quoted relative errors are due to statistics. There is an overall normalization error of  $\pm 8\%$  which is due mainly to the error in our measurement of the relative solid angle.

## DATA INTERPRETATION

The inelastic scattering data were fit with cross sections calculated in a distorted wave impulse approximation using the code DWPI.<sup>23</sup> The Kisslinger<sup>24</sup> and MSU potentials<sup>25,26</sup> were used to distort the incident and final pion wave functions. The Kisslinger potential strength parameters were obtained from best fits of our elastic scattering data<sup>7</sup> while the MSU potential is a prediction based on pionic atom data with a theoretical extension to finite energies. At low energies ( $\leq 50$  MeV) the MSU potential produces elastic scattering cross sections in reasonable agreement with the data. At 80 MeV the effects of the (3,3) resonance are important and it is not surprising that the elastic scattering cross sections predicted by the MSU potential are in poor agreement with the data. The parameters of each potential are given in Table II.

One additional parameter,  $\beta_L$  ( $L$  = orbital angular momentum of the excited state), which characterizes the coupling of the ground state to the excited state is needed to calculate inelastic cross sec-

TABLE I. 80 MeV  $\pi A$  inelastic scattering. (Errors shown are relative errors due to statistics. There is an overall normalization error of  $\pm 8\%$ .)

$^{12}\text{C}$ ( $2^+$ , 4.44 MeV)			$^{40}\text{Ca}$ ( $3^-$ , 3.7 MeV)		
$\theta_{\text{c.m.}}$ (deg)	$\frac{d\sigma(\pi^+)}{d\Omega_{\text{c.m.}}}$ (mb/sr)	$\frac{d\sigma(\pi^-)}{d\Omega_{\text{c.m.}}}$ (mb/sr)	$\theta_{\text{c.m.}}$ (deg)	$\frac{d\sigma(\pi^+)}{d\Omega_{\text{c.m.}}}$ (mb/sr)	$\frac{d\sigma(\pi^-)}{d\Omega_{\text{c.m.}}}$ (mb/sr)
55.9		0.45 $\pm$ 0.06	50.3	0.90 $\pm$ 0.08	
61.0		0.25 $\pm$ 0.04	60.3	0.53 $\pm$ 0.02	1.06 $\pm$ 0.12
66.0		0.18 $\pm$ 0.03	65.3		0.71 $\pm$ 0.09
81.1	0.55 $\pm$ 0.04		70.3	0.40 $\pm$ 0.02	
86.1		0.41 $\pm$ 0.04	75.3	0.44 $\pm$ 0.04	0.72 $\pm$ 0.07
91.1	0.64 $\pm$ 0.05	0.62 $\pm$ 0.05	80.3	0.57 $\pm$ 0.02	0.77 $\pm$ 0.06
96.1	0.83 $\pm$ 0.06	0.81 $\pm$ 0.06	85.3	0.82 $\pm$ 0.05	1.01 $\pm$ 0.08
101.1	1.07 $\pm$ 0.07	1.18 $\pm$ 0.07	90.3	1.04 $\pm$ 0.04	1.30 $\pm$ 0.09
106.1	1.35 $\pm$ 0.07	1.45 $\pm$ 0.08	95.3	1.30 $\pm$ 0.07	1.44 $\pm$ 0.10
111.1	1.63 $\pm$ 0.08	1.70 $\pm$ 0.08	100.3	1.69 $\pm$ 0.05	1.56 $\pm$ 0.11
116.0	1.63 $\pm$ 0.09	1.82 $\pm$ 0.07	105.3	1.83 $\pm$ 0.12	1.60 $\pm$ 0.11
121.0	1.71 $\pm$ 0.07	2.03 $\pm$ 0.09	110.3	1.91 $\pm$ 0.06	1.62 $\pm$ 0.12
125.9	1.84 $\pm$ 0.07	2.22 $\pm$ 0.10	115.3	1.96 $\pm$ 0.09	1.56 $\pm$ 0.15
			120.3	2.11 $\pm$ 0.06	1.71 $\pm$ 0.11
			125.3	2.00 $\pm$ 0.14	1.89 $\pm$ 0.13
$^{40}\text{Ca}$ (13.4 MeV)			$^{40}\text{Ca}$ (17.5 MeV)		
$\theta_{\text{c.m.}}$ (deg)	$\frac{d\sigma(\pi^+)}{d\Omega_{\text{c.m.}}}$ (mb/sr)	$\frac{d\sigma(\pi^-)}{d\Omega_{\text{c.m.}}}$ (mb/sr)	$\theta_{\text{c.m.}}$ (deg)	$\frac{d\sigma(\pi^+)}{d\Omega_{\text{c.m.}}}$ (mb/sr)	$\frac{d\sigma(\pi^-)}{d\Omega_{\text{c.m.}}}$ (mb/sr)
50.3	0.09 $\pm$ 0.14		50.3	0.21 $\pm$ 0.14	
60.3	0.03 $\pm$ 0.05		60.3	0.14 $\pm$ 0.11	
70.3	$\leq 0.006$		70.3	0.19 $\pm$ 0.10	
80.3	0.09 $\pm$ 0.03		80.3	0.30 $\pm$ 0.09	
90.3	0.08 $\pm$ 0.04	$\leq 0.04$	90.3	0.37 $\pm$ 0.18	$\leq 0.26$
100.3	0.15 $\pm$ 0.05		100.3	0.47 $\pm$ 0.14	
110.3	0.12 $\pm$ 0.08	0.22 $\pm$ 0.08	110.3	1.00 $\pm$ 0.23	0.74 $\pm$ 0.22
120.3	0.22 $\pm$ 0.08		120.3	0.78 $\pm$ 0.33	

tions. Often in the literature the deformation length  $\delta_L = \beta_L R$  is cited instead of  $\beta_L$ , where  $R$  is the radius obtained from an equivalent uniform density and is related to the root mean square matter density radius,  $R = (\frac{5}{3} \langle r^2 \rangle_{\text{matter}})^{1/2}$ . Our values of  $R$  for  $^{12}\text{C}$  and  $^{40}\text{Ca}$  are 3.1 and 4.4 fm, respectively. In this calculation the magnitude of the cross section is proportional to  $\beta_L^2$ . A full discussion of the meaning of  $\beta_L$  and its relation to the scattering of various probes from nuclei can be found in Ref. 22.

For  $^{12}\text{C}$  (Fig. 4) the  $\pi^+$  and  $\pi^-$  cross sections for excitation of the 4.44 MeV ( $2^+$ ) state have similar magnitudes at large angles. Using the expected  $\beta_2$  value of  $\sim 0.6$  (Refs. 27 and 28) results in poor fits for the Kisslinger potential (dashed curves). For  $\beta_2 = 0.6$  the MSU potential (solid curves) provides a

better representation of the data than the Kisslinger potential even though the Kisslinger potential gives a much better representation of the elastic scattering data. This appears to indicate that inelastic and elastic scattering are sensitive to different parts of the  $\pi A$  reaction mechanism. Best Kisslinger fits result for  $\beta_2$  values of 0.78 for  $\pi^+$  and 0.82 for  $\pi^-$ , somewhat higher than expected.

In the case of  $^{40}\text{Ca}$  (Fig. 5) the  $\pi^+$  and  $\pi^-$  cross sections for excitation of the 3.7 MeV ( $3^-$ ) state have similar values in the backward direction. In the forward direction the  $\pi^-$  cross sections are higher, in agreement with the simple arguments concerning Coulomb interference previously given. Both potentials predict deeper minima than are indicated by the data. Neither potential provides a good representation of the data except for  $\pi^+$

TABLE II. Optical potential parameters. These parameters are defined in Refs. 1, 25, and 26.

Kisslinger potential		
$^{12}\text{C}$ , 80 MeV,	$\pi^+$ : $b_0 = -1.85 - 0.85i$ ,	$b_1 = 6.21 + 2.18i$
	$\pi^-$ : $b_0 = -1.61 - 1.17i$ ,	$b_1 = 6.62 + 2.22i$
matter density $\rho(r) \propto \{1 + \exp[(r - 2.5 \text{ fm})/0.37 \text{ fm}]\}^{-1}$		
$^{40}\text{Ca}$ , 80 MeV,	$\pi^+$ : $b_0 = -2.83 - 0.81i$ ,	$b_1 = 7.88 + 2.53i$
	$\pi^-$ : $b_0 = -2.72 - 0.95i$ ,	$b_1 = 7.48 + 1.77i$
$^{40}\text{Ca}$ , 65 MeV,	$\pi^+$ : $b_0 = -2.90 - 0.56i$ ,	$b_1 = 6.71 + 1.98i$
matter density $\rho(r) \propto \{1 + \exp[(r - 3.63 \text{ fm})/0.51 \text{ fm}]\}^{-1}$		
MSU potential		
80 MeV	$b_0 = -0.07 + 0.0107i$ ,	$c_0 = 0.82 + 0.1034i$
	$B_0 = -0.04 + 0.18i$ ,	$C_0 = 0.48 + 0.92i$
	$b_1 = -0.13$ ,	$c_1 = 0.46 + 0.05i$
	$\lambda = 1.0$	
Matter densities:	$^{12}\text{C}\rho(r) \propto [1 + 1.33(r/1.57 \text{ fm})^2]/\exp(r/1.57 \text{ fm})^2$	
	$^{40}\text{C}\rho(r) \propto \{1 + \exp[(r - 3.51 \text{ fm})/0.563 \text{ fm}]\}^{-1}$	

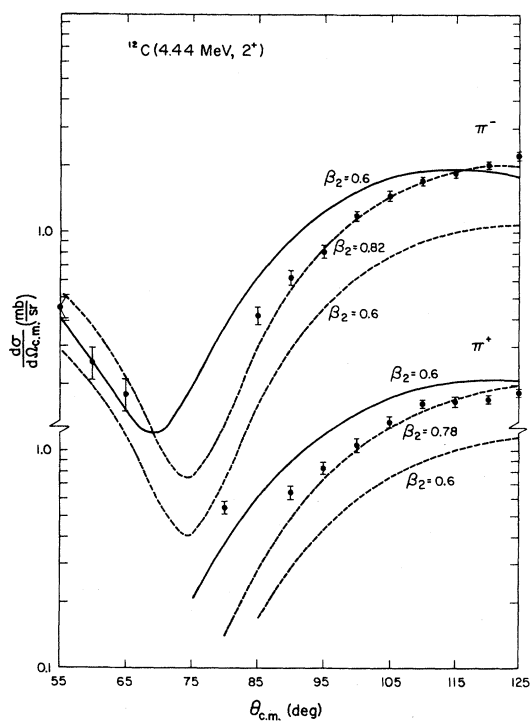


FIG. 4. Cross sections for scattering to the 4.44 MeV ( $2^+$ ) state in  $^{12}\text{C}$ . Solid curves are for the MSU potential. Dashed curves are for the Kisslinger potential. The curves are labeled by the deformation parameter  $\beta_2$ .

scattering at backward angles where the Kisslinger potential (dashed curve) does very well. Best Kisslinger fits result for  $\beta_3$  values of 0.5 for  $\pi^+$  and 0.56 for  $\pi^-$  somewhat higher than the expected value of  $\sim 0.4$ .<sup>29</sup> Inasmuch as excitation of the 3.9 MeV ( $2^+$ ) state could not be experimentally separated from the 3.7 MeV ( $3^-$ ) state we fit the cross sections for scattering from  $^{40}\text{Ca}$  assuming  $2^+$  excitation. The resulting curves give much worse  $\chi^2$  (a factor of 10), indicating mainly  $3^-$  excitation. This result is expected since other studies<sup>29</sup> have found  $(\beta_3/\beta_2)^2 \sim 16$ .

The  $\pi^+$  angular distributions for excitation of high-lying states at 13.4 and 17.5 MeV in  $^{40}\text{Ca}$  are plotted in Fig. 6. As previously discussed these states are only weakly excited above the background. Thus a small uncertainty in the shape or magnitude of the background produces a large uncertainty in the cross sections which is reflected in the large error bars shown on the data. This is especially the case for the 13.4 MeV state. At  $90^\circ$  and  $110^\circ$  these states were observed with a  $\pi^-$  probe. Within the experimental errors the cross sections are the same as the  $\pi^+$  cross sections. The curves are fits to the structureless  $\pi^+$  angular distributions using DWPI. Kisslinger potential strength parameters for the final state were taken from our 65 MeV elastic scattering data<sup>6</sup> (see Table II).

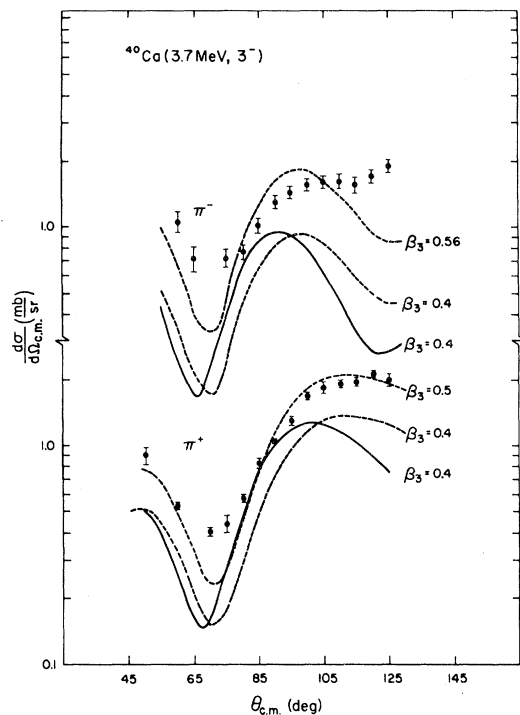


FIG. 5. Cross sections for scattering to the 3.7 MeV ( $3^-$ ) state in  $^{40}\text{Ca}$ . Solid curves are for the MSU potential, dashed curves are for the Kisslinger potential. The curves are labeled by the deformation parameter  $\beta_3$ .

For the 17.5 MeV state which has previously been identified as a giant quadrupole resonance (GQR) (Ref. 22) only  $L=2$  was assumed. From the best fit to the data  $\beta_2=0.26$  was obtained. This value of  $\beta_2$  is equivalent to the depletion of  $100 \pm 30\%$  of the  $I=0, L=2$  energy weighted sum rule (EWSR),<sup>22</sup> where a radius of 4.4 fm is used (see earlier discussion). This value is approximately twice as large as that deduced from proton and  $\alpha$  particle inelastic scattering,<sup>22</sup> but in agreement with that deduced from  $\pi$  inelastic scattering.<sup>15</sup> The most likely cause of this discrepancy is in the uncertainty in the potential parameters used to describe  $\pi$  inelastic scattering. Including the data presented in this paper there are few results available for excitation of low-lying states where the DWPI calculation can be checked.

For the 13.4 MeV state both  $L=0$  and  $L=2$  assignments were assumed because studies of  $(\alpha, \alpha')$  (Refs. 30 and 31) and  $(^3\text{He}, ^3\text{He}')$  reactions<sup>32</sup> have observed such states in this excitation energy region. The  $(\alpha, \alpha')$  measurements of Ref. 30 indicated a  $2^+$  assignment for the state, while that of Ref. 31 found both a  $0^+$  and a  $2^+$  state in this excitation re-

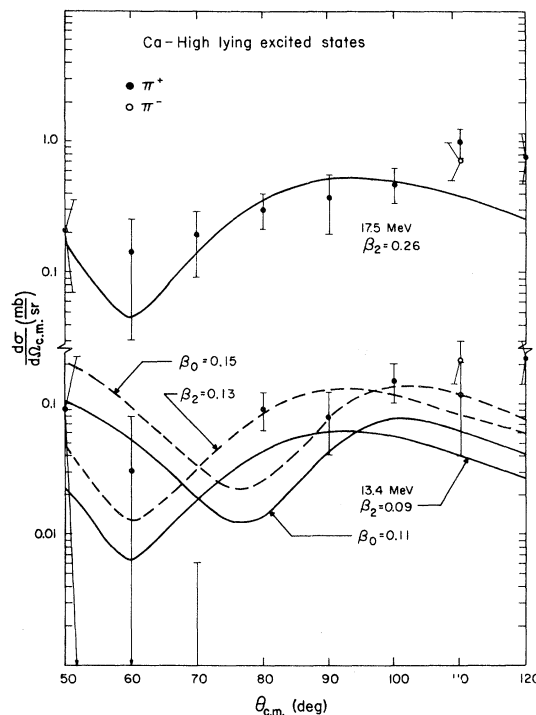


FIG. 6. Cross sections for scattering from high-lying excited states at 13.4 and 17.5 MeV in  $^{40}\text{Ca}$ . The curves are best fits to the data using a Kisslinger potential. For the state at 17.5 MeV  $L=2$  was assumed. For the state at 13.4 MeV both  $L=0$  and  $L=2$  were assumed. The dashed curves are best fits obtained when the  $70^\circ$  cross section is excluded from the data.

gion. The  $(^3\text{He}, ^3\text{He}')$  measurements suggested a  $0^+$  assignment for the state.

In Fig. 6 the solid (dashed) curves are best fits to the data which include (exclude) the  $70^\circ$  cross section. Although the results are marginally better described by the  $L=2$  calculation no definite assignment can be made because of the large cross section uncertainties. The complete angular distribution for an  $L=2$  assignment yields an EWSR depletion of 10–30%, while the  $L=0$  calculation implies 20–40% depletion of the monopole sum rule. As was the case for the 17.5 MeV state, the EWSR depletion deduced for the 13.4 MeV state, if  $2^+$ , is considerably larger than the depletion obtained from the  $(\alpha, \alpha')$  measurements.<sup>30,31</sup>

## SUMMARY

We have observed with 80 MeV  $\pi^\pm$  inelastic  $\pi A$  scattering from the 4.44 MeV ( $2^+$ ) state of  $^{12}\text{C}$ , and the 3.7 MeV ( $3^-$ ) state of  $^{40}\text{Ca}$ . The inelastic cross

sections are not well fit using a Kisslinger potential, which fits the elastic scattering data, and a deformation parameter  $\beta_L$  obtained from inelastic scattering experiments using projectiles other than pions. In the case of  $^{12}\text{C}$  and  $^{40}\text{Ca}$  ( $\pi^+$ ) variation of the deformation parameter  $\beta_L$  allows good fits to be obtained. The best fit values of  $\beta_L$  are 25 to 35 % higher than expected. Excitation of a giant quadrupole resonance at 17.5 MeV in  $^{40}\text{Ca}$  is observed but the signal is weaker than at higher energies. This excitation appears to be equally excited at  $90^\circ$  and  $110^\circ$  by  $\pi^+$  and  $\pi^-$  probes. A state at excitation energy 13.4 MeV is also observed and is reasonably fit with an  $L=2$  assumption. It too is equally excited by  $\pi^+$  and  $\pi^-$  at  $90^\circ$  and  $110^\circ$ .

#### ACKNOWLEDGMENTS

We thank the Los Alamos National Laboratory (LANL) for the technical help provided us. We are indebted to H. McManus who provided us with his optical model calculations of the cross sections, and for illuminating comments. This work was supported by the National Science Foundation (Virginia Polytechnic Institute and State University and the University of South Carolina) and the Department of Energy (MIT, LAMPF), and the Oak Ridge National Laboratory—through the Union Carbide Corporation under the DOE Contract (W-7405-eng-2).

- <sup>1</sup>B. M. Preedom, in *Proceedings of the 7th International Conference on High Energy Physics and Nuclear Structure, Zurich (1977)*, edited by M. P. Locher (Birkhauser, Basel, 1977).
- <sup>2</sup>R. P. Redwine, in AIP Conference Proceedings No. 54, *Meson-Nuclear Physics—1979 (Houston)*, Proceedings of the 2nd International Topical Conference on Meson-Nuclear Physics, edited by E. V. Hungerford III (AIP, New York, 1979), p. 501.
- <sup>3</sup>S. A. Dytman, J. F. Amann, P. D. Barnes, J. N. Craig, K. G. R. Doss, R. A. Eisenstein, J. D. Sherman, W. R. Wharton, G. R. Burlinson, S. L. Verbeck, R. J. Peterson, and H. A. Thiessen, *Phys. Rev. C* **19**, 971 (1979).
- <sup>4</sup>M. Blecher, K. Gotow, D. Jenkins, F. Milder, F. E. Bertrand, T. P. Cleary, E. E. Gross, C. A. Ludemann, M. A. Moinester, R. L. Burman, M. Hamm, R. P. Redwine, M. Yates-Williams, S. Dam, C. W. Darden III, R. D. Edge, D. J. Malbrough, T. Marks, and B. M. Preedom, *Phys. Rev. C* **20**, 1884 (1979).
- <sup>5</sup>B. Preedom, S. H. Dam, C. W. Darden III, R. D. Edge, D. J. Malbrough, T. Marks, R. L. Burman, M. Hamm, M. A. Moinester, R. P. Redwine, M. A. Yates, F. E. Bertrand, T. P. Cleary, E. E. Gross, N. W. Hill, C. A. Ludemann, M. Blecher, K. Gotow, D. Jenkins, and F. Milder, *Phys. Rev. C* **23**, 1134 (1981).
- <sup>6</sup>S. H. Dam, R. D. Edge, B. M. Preedom, F. E. Bertrand, E. E. Gross, M. Blecher, K. Gotow, R. L. Burman, R. Carlini, M. E. Hamm, R. P. Redwine, M. A. Yates-Williams, and M. A. Moinester, see Ref. 2, p. 525; and *Phys. Rev. C* (to be published).
- <sup>7</sup>M. Blecher, R. Auble, F. E. Bertrand, W. Bertozzi, G. Blanpied, R. L. Burman, R. Carlini, S. Dam, W. Gaskin, K. Gotow, E. E. Gross, M. V. Hynes, M. A. Kovash, M. J. Leitch, F. E. Obenshain, B. M. Preedom, R. P. Redwine, B. G. Ritchie, V. Sandberg, and J. Wu, *Proceedings of the 9th International Conference on High Energy Physics and Nuclear Structure, Versailles, France, 1981*; and *Phys. Rev. C* (to be published).
- <sup>8</sup>F. E. Obenshain, F. E. Bertrand, M. Blecher, R. L. Burman, R. D. Edge, K. Gotow, E. E. Gross, M. Hamm, M. J. Leitch, M. A. Moinester, B. M. Preedom, R. P. Redwine, and J. R. Wu, *Proceedings of the 9th International Conference on High Energy Physics and Nuclear Structure, Versailles, France, 1981*; and *Phys. Rev. C* (to be published).
- <sup>9</sup>For example, C. A. Wiedner, J. A. Nolen, Jr., W. Saathoff, R. E. Tribble, J. Bolger, J. Zichy, K. Stricker, H. McManus, and J. A. Carr, *Phys. Lett.* **78B**, 26 (1978).
- <sup>10</sup>R. J. Peterson, in *Proceedings of the 8th International Conference on High Energy Physics and Nuclear Structure, Vancouver, Canada*, edited by D. F. Measday and A. W. Thomas, *Nucl. Phys.* **A335**, 365 (1980).
- <sup>11</sup>F. E. Bertrand, see Ref. 2, p. 230.
- <sup>12</sup>H. A. Thiessen, in *Proceedings of the 8th International Conference on High Energy Physics and Nuclear Structure, Vancouver, Canada, 1979*, edited by D. F. Measday and A. W. Thomas, *Nucl. Phys.* **A335**, 339 (1980).
- <sup>13</sup>C. H. Q. Ingram, see Ref. 2, p. 455.
- <sup>14</sup>J. F. Amann, P. D. Barnes, K. G. R. Doss, S. A. Dytman, R. A. Eisenstein, J. D. Sherman, and W. R. Wharton, *Phys. Rev. C* **23**, 1635 (1981).
- <sup>15</sup>J. Arvieux, J. P. Albanese, M. Buenerd, D. Lebrun, E. Boschitz, C. H. Q. Ingram, and J. Jansen, *Phys. Rev. Lett.* **42**, 753 (1979).
- <sup>16</sup>D. Chiang, K. Aniol, I. Halpern, P. Barnes, K. Doss, S. Dytman, R. Eisenstein, C. Ellegaard, F. Takeuchi, W. Wharton, J. Amann, M. Cooper, and L. Knutson, in *Proceedings of the 8th International Conference on High Energy Physics and Nuclear Structure, Vancouver, Canada, 1979*, edited by D. F. Measday and A. W. Thomas, Abstracts p. 51. See also the discussion of this giant resonance data in Ref. 11.
- <sup>17</sup>F. Milder, M. Blecher, K. Gotow, D. Jenkins, P. Roberson, R. L. Burman, M. A. Moinester, R. P. Redwine, F. E. Bertrand, T. P. Cleary, E. E. Gross, C. A. Ludemann, C. W. Darden III, R. E. Edge, D. Mal-



- brough, T. Marks, and B. M. Freedom, *Phys. Lett.* **72B**, 159 (1977).
- <sup>18</sup>A. E. S. Green, R. J. Berkley, C. E. Watson, and C. F. Moore, *Rev. Sci. Instrum.* **37**, 415 (1966).
- <sup>19</sup>W. Bertozzi, M. V. Hynes, C. P. Sargent, C. Creswell, P. C. Dunn, A. Hirsch, M. Leitch, B. Norum, F. N. Rad, and T. Sasanuma, *Nucl. Instrum. Methods* **141**, 457 (1977).
- <sup>20</sup>P. Y. Bertin, B. Coupat, A. Hivernat, D. B. Isabelle, J. Duclos, A. Gerard, J. Miller, J. Morgenstern, J. Picard, J. Vernin, and R. Powers, *Nucl. Phys.* **B106**, 341 (1976).
- <sup>21</sup>V. S. Zidell, R. A. Arndt, and L. D. Roper, *Phys. Rev. D* **21**, 1255 (1980).
- <sup>22</sup>F. E. Bertrand, *Annu. Rev. Nucl. Sci.* **26**, 457 (1976).
- <sup>23</sup>R. A. Eisenstein and G. A. Miller, *Comput. Phys. Commun.* **11**, 95 (1976).
- <sup>24</sup>L. S. Kisslinger, *Phys. Rev.* **98**, 761 (1955).
- <sup>25</sup>K. Stricker, J. A. Carr, and H. McManus, *Phys. Rev. C* **22**, 2043 (1980).
- <sup>26</sup>K. Stricker, H. McManus, and J. A. Carr, *Phys. Rev. C* **19**, 929 (1979).
- <sup>27</sup>R. M. Haybron, M. B. Johnson, and R. J. Metzger, *Phys. Rev.* **156**, 1136 (1967).
- <sup>28</sup>G. S. Blanpied, G. W. Hoffman, M. L. Barlett, J. A. McGill, S. J. Greene, L. Ray, O. B. Van Dyck, J. Amann, and H. A. Thiessen, *Phys. Rev. C* **23**, 2599 (1981).
- <sup>29</sup>Reference 15 gives a value of  $\beta_3=0.47$ , C. R. Gruhn, T. Kuo, C. J. Maggiore, H. McManus, F. Petrovich, and B. M. Freedom, *Phys. Rev. C* **6**, 915 (1972), gives a  $\delta_3=1.36$  fm for a radius of 3.96 fm. Using the same  $\delta_3$  and our radius yields  $\beta_3=0.31$ . Electron scattering data can also yield  $\beta_L$  values. Using formula 6 of Ref. 22, the results of R. A. Eisenstein, D. W. Madsen, H. Theissen, L. S. Cardman, and C. K. Bockelman, *Phys. Rev.* **188**, 1815 (1969) yield  $\beta_3=0.36$ ,  $(\beta_3/\beta_2)^2 \sim 16$ .
- <sup>30</sup>D. H. Youngblood, A. D. Bacher, D. R. Brown, J. D. Bronson, J. M. Moss, and C. M. Rozsa, *Phys. Rev. C* **15**, 246 (1977).
- <sup>31</sup>Y. W. Lui, J. D. Bronson, C. M. Rozsa, D. H. Youngblood, P. Bogucki, and U. Garg, *Phys. Rev. C* **24**, 884 (1981).
- <sup>32</sup>T. Yamagata, K. Iwamoto, S. Kishimoto, B. Saeki, K. Yuasa, M. Tanaka, T. Fukuda, K. Okada, L. Miura, M. Inoue, and H. Ogata, *Phys. Rev. Lett.* **40**, 1628 (1978).